nature COMMUNICATIONS

ARTICLE

Received 5 Jul 2016 | Accepted 10 Jan 2017 | Published 27 Feb 2017

DOI: 10.1038/ncomms14546 OPEN

Canonical free-energy barrier of particle and polymer cluster formation

Johannes Zierenberg[1], Philipp Schierz[1] & Wolfhard Janke[1]

A common approach to study nucleation rates is the estimation of free-energy barriers. This usually requires knowledge about the shape of the forming droplet, a task that becomes notoriously difficult in macromolecular setups starting with a proper definition of the cluster boundary. Here we demonstrate a shape-free determination of the free energy for temperature-driven cluster formation in particle as well as polymer systems. Combined with rigorous results on equilibrium droplet formation, this allows for a well-defined finite-size scaling analysis of the effective interfacial free energy at a fixed density. We first verify the theoretical predictions for the formation of a liquid droplet in a supersaturated particle gas by generalized-ensemble Monte Carlo simulations of a Lennard-Jones system. Going one step further, we then generalize this approach to cluster formation in a dilute polymer solution. Our results suggest an analogy with particle condensation, when the macromolecules are interpreted as extended particles.

[1] Institut für Theoretische Physik, Universität Leipzig, Postfach 100 920, D-04009 Leipzig, Germany. Correspondence and requests for materials should be addressed to J.Z. (email: johannes.zierenberg@itp.uni-leipzig.de) or to P.S. (email: philipp.schierz@itp.uni-leipzig.de) or to W.J. (email: wolfhard.janke@itp.uni-leipzig.de).

The formation of equilibrium droplets from a supersaturated gas is a long-standing subject of interest, being an essential phase transition in nature[1–3]. More importantly, the underlying mechanism is relevant for a multitude of nucleation-like processes from statistical mechanics to material science. These include crystallization in colloidal suspensions[4,5] and cluster formation in protein solutions[5,6], as well as domain formation in so-called phase-change materials[7–9] and glassy solids[10]. It is even connected to field theory[11] and nuclear reactions[12]. The formal framework of free-energy calculations is straightforward, for example, in terms of reaction coordinates in phase space, but the application in computer simulations is diverse with an ongoing demand for further methodological developments[13]. A seminal application was the parameter-free estimate of crystal nucleation rates from equilibrium free-energy barriers[4]. It seems natural that the estimation of nucleation barriers becomes increasingly difficult when considering more complex systems, such as polymer or protein solutions[5].

The rate of nucleation R is related by classical nucleation theory[1,3] to the free-energy cost $\beta\Delta F$ of a nucleus on top of the nucleation barrier:

$$R=\kappa e^{-\beta\Delta F}, \tag{1}$$

with the inverse temperature $\beta=1/k_{\mathrm{B}}T$ and the Boltzmann constant k_{B}. The kinetic prefactor κ includes the kinetic details of the nucleation process, such as diffusion and nucleus-attachment rates. The free-energy barrier may be related to the suppression in the equilibrium probability distribution. Physically relevant barriers for liquid-vapour condensation are supposed to be in the range of $20k_{\mathrm{B}}T$ to $100k_{\mathrm{B}}T$ (see, for example, ref. 14). The typical setup for the study of free-energy barriers is at fixed temperature by variation of the density or degree of supersaturation or directly in the grand canonical ensemble. The barrier is then associated with the suppression in the droplet-size probability distribution[4] and is clearly temperature dependent[15,16]. This usually requires estimating the droplet size and interface, a task that introduces systematic uncertainties and strongly depends on the droplet definition. Instead, the free-energy barrier may be directly related to the volume of the critical nucleus and the pressure difference[17], exploiting a thorough understanding of the underlying phenomenon in a clever way. In this context, the problem can be reduced to conformational phase space, knowing that canonical expectation values typically do not depend on the kinetic energy.

In the following, we address the question of how to easily obtain dependable results on nucleation barriers without invoking elaborate thermodynamic reasoning or estimating nucleus shapes. This opens the door to more complex systems with nucleation-like mechanisms such as self-assembly and aggregation, where the nucleus shapes are a priori unknown. Importantly, we consider a setup at fixed density with varying temperature—an intuitive approach from a condensed matter perspective. We focus on aggregation of polymers in a dilute setup[18–20] guided by the canonical case of droplet formation in a particle gas. For the canonical case, we analyse a two-dimensional free-energy landscape and identify the energy as a suitable reaction coordinate. This allows us to formulate the problem in the microcanonical ensemble of either fixed total energy E or fixed potential energy E_{p}. The first is the usual textbook definition, while the latter has been frequently applied in recent computer simulation studies. This enables us to directly discuss the effect of kinetic energy when changing between the two formulations $E\leftrightarrow E_{\mathrm{p}}$. If kinetic energy matters, only the first one allows a direct physical interpretation.

Results

Droplet formation free-energy barrier. We begin with the paradigm of nucleation and dissolution, the equilibrium droplet formation in a supersaturated particle gas[21–29]. The first-order condensation–evaporation transition separates a homogeneous gas phase from an inhomogeneous phase, where a single macroscopic droplet of size N_{D} is in equilibrium with the remaining vapour[21–26]. In fact, the probability for intermediate-sized droplets was shown to vanish[23,24]. In the vicinity of the transition, the energy-dominated inhomogeneous condensed phase coexists with the entropy-dominated homogeneous gas phase. A transition between both phases may only occur by energy variation upon nucleation or dissolution. In reality, this of course refers to the total energy E. For systems where the momentum phase space may be integrated out explicitly (see Methods section), the problem simplifies in terms of computability. We hence begin with an illustration in the potential energy formulation (denoted by a hat, for example, $\hat{F}$) as a direct result of computer simulations before we go over to comparing both energy approaches.

Figure 1a shows the free-energy landscape $\beta\hat{F}(E_{\mathrm{p}},N_{\mathrm{D}})$ of droplet condensation–evaporation of Lennard-Jones particles (see Methods section) at the finite-size transition temperature. We define $\beta\hat{F}(E_{\mathrm{p}},N_{\mathrm{D}})=-\ln\left[\Omega(E_{\mathrm{p}},N_{\mathrm{D}})e^{-\beta E_{\mathrm{p}}}\right]$, where $\Omega(E_{\mathrm{p}},N_{\mathrm{D}})$ is a generalization of the (conformational) density of states to the two-dimensional E_{p}–N_{D} reaction coordinate space. For E_{p} fixed, $\beta\hat{F}(E_{\mathrm{p}},N_{\mathrm{D}})$ resembles a parabola with a single local minimum. The resulting transition path is shown as a black line and its relative maximum along this path (around E_{p}^{0}) is an estimate of the transition free-energy barrier. Instead, however, one may consider the projection along the droplet size[4] or equivalently along the energy, connected to the corresponding probability distributions $\beta\hat{F}(N_{\mathrm{D}})=-\ln\hat{P}_{\beta}(N_{\mathrm{D}})$ and $\beta\hat{F}(E_{\mathrm{p}})=-\ln\hat{P}_{\beta}(E_{\mathrm{p}})$.

We follow the latter approach and derive the free-energy barrier from the suppression of transition states in the canonical energy probability distributions (see Methods section) for both reaction coordinates E and E_{p}. The probability distributions are shown in Fig. 1b,d and are clearly asymmetric, with a narrow peak for the gas phase and a broad peak for the droplet phase. Methodologically, both ensembles are analogous so that we limit in the following the notation to the case of total energy E. At the equal-height inverse temperature β_{eqh}, $P_{\beta_{\mathrm{eqh}}}(E)$ has two peaks at $E^{\pm}$ of equal height and in between a minimum at E^{0}. The resulting free-energy barrier is $\beta\Delta F=\ln(P_{\beta_{\mathrm{eqh}}}(E^{\pm})/P_{\beta_{\mathrm{eqh}}}(E^{0}))$. Equivalently, one may perform the analysis entirely in the microcanonical frame[30] and consider the enclosed area by the microcanonical inverse temperature $\beta(E)$ and the canonical inverse temperature (see Methods section)

$$\beta\Delta F=\int_{E^{0}}^{E^{\pm}}\mathrm{d}E\;[\beta(E)-\beta], \tag{2}$$

shown in Fig. 1c,e. Demanding areas of equal size yields the equal-area inverse temperature β_{eqa}, which is in fact identical to β_{eqh} (ref. 31).

We notice that the energy probability distributions $P_{\beta}(E)$ and $\hat{P}_{\beta}(E_{\mathrm{p}})$ are related by a convolution involving the Maxwell–Boltzmann distribution $P_{\mathrm{MB}}(x)$ as $P_{\beta}(E)=(\hat{P}_{\beta}\times P_{\mathrm{MB}})(E)$ (see Methods section). This in turn corresponds to a physical smoothing, which diminishes the ratio between maxima and minimum. As a consequence, we expect a lower barrier in the total energy formulation due to the kinetic contribution.

Finite-size scaling of free-energy barrier. In the following, we discuss the free-energy barrier of droplet formation in a particle gas and a dilute polymer solution as a function of system size. We

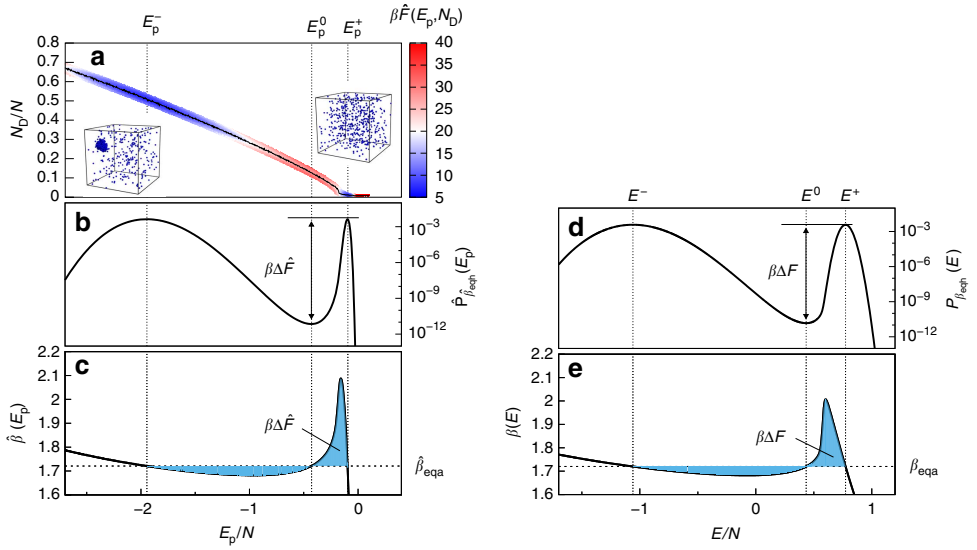

Figure 1 | Free-energy barrier of droplet formation. (**a**) Illustration of the free-energy landscape $\beta\hat{F}(E_p, N_D)$ (colour map) as a function of potential energy E_p and droplet size N_D for $N=512$ Lennard-Jones particles. The minimal free-energy path (black solid line) connects a droplet ($E_p \approx E_p^-$) and a gaseous ($E_p \approx E_p^+$) phase, visualized by the snapshots at $E_p^{\pm}$. (**b**) The projection onto the reaction coordinate E_p yields the canonical potential energy probability distribution $\hat{P}_\beta(E_p)$, where the free-energy barrier $\beta\Delta\hat{F}$ is encoded in the ratio between maximum and minimum at $\hat{\beta}_{eqh}$. (**c**) Equivalently, $\beta\Delta\hat{F}$ is the (equal) area size enclosed between the microcanonical inverse temperature $\hat{\beta}(E_p)$ and the accordingly defined transition temperature $\hat{\beta}_{eqa}$, where $\hat{\beta}_{eqa}=\hat{\beta}_{eqh}=1.72099(3)$. The analogous quantities are re-evaluated as a function of total energy E in panels (**d**,**e**) with $\beta_{eqa}=\beta_{eqh}=1.71999(3)$.

here extend the notion of droplet formation to the formation of clusters or aggregates in polymeric systems. In particular, we consider linear bead-spring polymers (see Methods section), each consisting of 13 monomers. The resulting polymer cluster or aggregate is coexisting with a polymer 'gas', see Fig. 2, a first sign for the analogy to particle droplet formation.

The free-energy barrier is commonly assumed to be proportional to the occurring interface. Here the surface of the droplet ∂V_D separates the liquid droplet from the surrounding gas and consequently we expect $\beta\Delta F=\sigma\partial V_D$, with the interface tension σ. For any non-fractal shape, the surface area is related to the droplet volume V_D as $\partial V_D \propto V_D^{2/3}$. Since nucleation shows no sign of critical behaviour, this is a physically valid assumption. However, at the condensation–evaporation transition V_D itself does not scale trivially with system size V. At a fixed temperature, general arguments exploiting the equivalence to the Ising model imply that droplet formation is triggered by insertion of particles until a single macroscopic droplet of size $V_D \propto V^{3/4}$ coexists with the surrounding vapour[23–26]. This result may be translated to a fixed-density setup using Taylor expansions, where directly at the finite-size transition temperature the analogue scaling $V_D \propto N^{3/4}$ was verified for both lattice and off-lattice particle models[29].

Putting everything together and introducing an effective interfacial free energy τ_{eff} then yields to leading order $\beta\Delta F \propto \tau_{eff} N^{1/2}$. It is common for the study of interface tensions to consider logarithmic corrections[32–35], dating back to early field theoretic results[11]. The physical origin are translational invariance as well as capillary waves at the interface. Altogether we use for our final scaling ansatz

$$\beta\Delta F = \tau_{eff} N^{1/2} - \alpha \ln N + c, \qquad (3)$$

where α and c are constants. This is the leading-order exponent in equation (1). Neglecting the prefactor κ for now, we obtain from equation (3) to leading order the rate of equilibrium droplet formation as $R \propto N^{\alpha} e^{-\tau_{eff} N^{1/2}}$. Thus for increasing system size the probability that a single macroscopic droplet forms decreases exponentially.

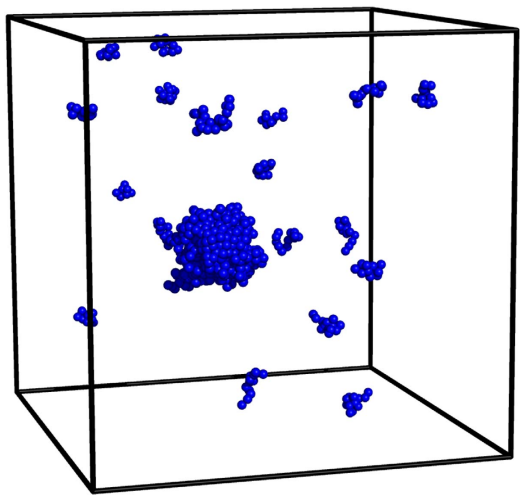

Figure 2 | Polymer aggregate in a dilute solution. Illustration of a cluster or aggregate of polymers in a dilute solution ($N=64$ bead-spring polymers with 13 monomers each; monomer density $\rho=10^{-2}$). The snapshot stems from the droplet phase ($E_p \approx E_p^-$).

Figure 3a shows the free-energy barrier for droplet formation in a particle gas as a function of system size for both reaction coordinates E and E_p, obtained via equation (2). Both estimates yield barriers up to about $42k_BT$, showing at close sight an almost constant shift. Only the total energy E includes the kinetic contribution, which is here reflected in a smaller barrier, whereas the interfacial free energies are expected to be identical, $\tau_{eff}=\hat{\tau}_{eff}$. In fact, fits to equation (3) yield $\tau_{eff}=0.939(4)$ and $\hat{\tau}_{eff}=0.935(4)$, each for $N \geq N_{min}=320$ with goodness-of-fit parameter $Q \approx 0.3$, for reaction coordinate E and E_p, respectively. This remains consistent within error bars under variation of $N_{min} \in [224, 1{,}280]$. The accordance of data and fit is demonstrated in the inset. In order to test the significance of the logarithmic corrections, we

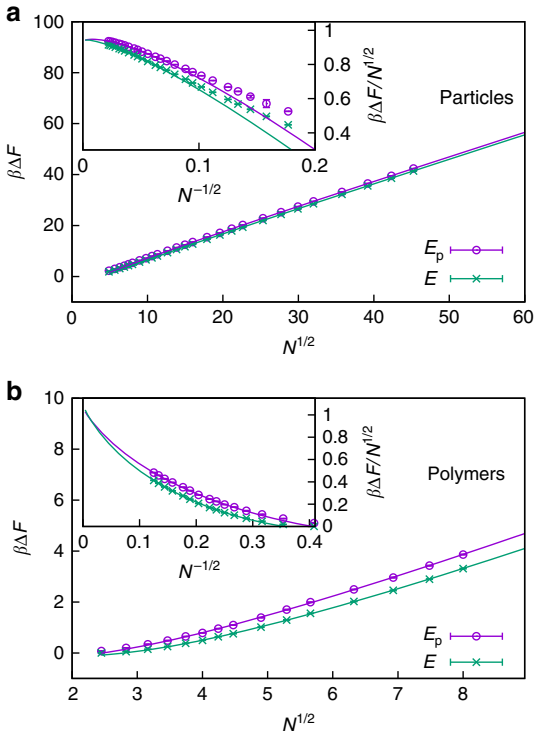

Figure 3 | Finite-size scaling of free-energy barrier. Free-energy barriers $\beta\Delta\hat{F}$ (reaction coordinate E_p) and $\beta\Delta F$ (reaction coordinate E) of droplet formation in a particle gas (**a**) and dilute polymer solution (**b**) as a function of the number of constituents N. The leading $N^{1/2}$ scaling is clearly demonstrated. The insets show the finite-size scaling of the interfacial free energy according to equation (3). Error bars indicate the s.e.m. obtained from Jackknife error analysis.

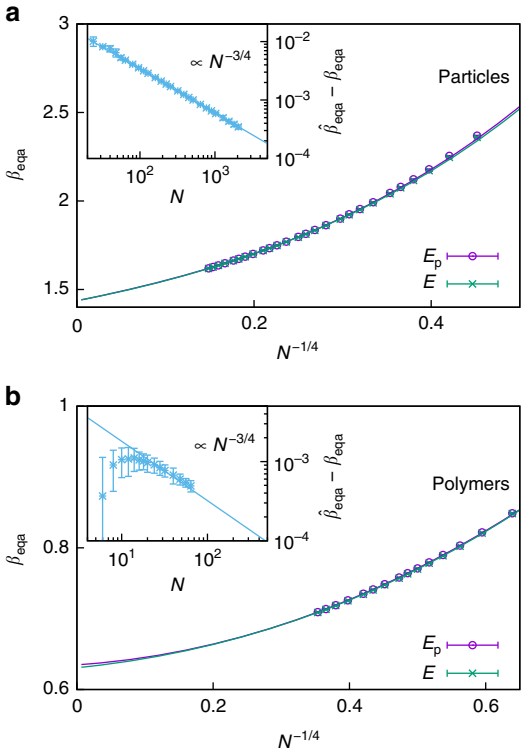

Figure 4 | Finite-size scaling of transition temperature. Inverse transition temperature $\hat{\beta}_{eqa}$ (reaction coordinate E_p) and β_{eqa} (reaction coordinate E) of droplet formation in a particle gas (**a**) and dilute polymer solution (**b**) as a function of the number of constituents N. The finite-size scaling ansatz of equation (4) describes the data perfectly. The inset shows a vanishing finite-size difference between both ensembles $\hat{\beta}_{eqa}(N)-\beta_{eqa}(N)\propto N^{-3/4}$. Error bars indicate the s.e.m. obtained from Jackknife error analysis.

considered in addition a restricted fit to $\beta\Delta F=\tau_{eff}N^{1/2}+c$. We obtain $\tau_{eff}=0.973(2)$ and $\hat{\tau}_{eff}=0.977(2)$ for $N_{min}=768$ with $Q\approx0.2$ and $Q\approx0.1$, respectively. However, the estimate of τ_{eff} gradually decreases with increasing N_{min}. Thus the most probable scenario remain small logarithmic corrections competing with a constant shift. The leading scaling behaviour was also observed in ref. 17 directly as a linear function of the droplet surface. The advantage of the present approach is that it avoids difficulties and uncertainties coming from the 'correct' identification of the cluster surface.

For the cluster formation in a dilute polymer solution shown in Fig. 3b, the situation remains qualitatively similar. Fits to equation (3) yield $\tau_{eff}=1.06(3)$ and $\hat{\tau}_{eff}=1.03(3)$, each for $N_{min}=16$ with $Q\approx0.2$, for reaction coordinate E and E_p, respectively. Note that this is on the same scale as for droplet formation of particles in Fig. 3a. Compared with the particle case, the system sizes are, however, much smaller, making quantitative predictions for the polymer case less reliable. Still, the overall behaviour supports the hypothesis that cluster formation in a dilute polymer solution shows a strong analogy to droplet formation in a particle gas.

We observe that considering the kinetic contribution results in a shifted barrier. For the considered examples and relevant system sizes, the shift is about $\beta\Delta\hat{F}-\beta\Delta F\approx 0.5\ldots1$, that is, of the order $\mathcal{O}(1)$. This additive contribution, while much smaller than the leading behaviour, leads to a multiplicative relation between the nucleation rates $R\propto e^{-\beta\Delta F}\approx e^{-(\beta\Delta\hat{F}-1)}\approx 3e^{-\beta\Delta\hat{F}}\propto 3\hat{R}$. Neglecting the momentum phase space thus underestimates the rates. In common situations, however, the deviations between experiment and simulations are of the order of several magnitudes, such that the effect of the kinetic contribution may be considered subleading.

Finite-size scaling of transition temperature. The evaluation of the free-energy barrier via equal areas provides us with a definition of the finite-size transition temperature. At fixed density, we showed for the condensation–evaporation transition[29] that the transition temperature, obtained from specific-heat peaks, scales as inverse power of the critical droplet radius $R_D\propto V_D^{1/3}\propto N^{1/4}$. The same is expected for all other transition temperature definitions. Figure 4 shows the equal-area definition together with a fit including higher-order corrections of the form

$$\beta_{eqa}(N)=\beta_0+aN^{-1/4}+bN^{-1/2}+cN^{-3/4}, \qquad (4)$$

for cluster formation in both particle gas and polymer solution. In the case of particle condensation, least-square fits for $N_{min}=192$ yield $\beta_0=1.436(2)$ and $\hat{\beta}_0=1.436(2)$ each with $Q\approx0.5$, for reaction coordinate E and E_p, respectively. The excellent fit results show that the empirical, yet physically motivated, higher-order corrections describe the finite-size scaling very well. In addition, the strong finite-size deviations open a possibility to study finite-size scaling in experiments on the nanoscale (for a conversion, see Methods section). The finite-size transition temperature of the largest system ($N=2{,}048$) is $\beta_{eqa}\sim1.61948(2)$, which still deviates from the thermodynamic limit by $\mathcal{O}(10\%)$.

It is worth noting that typical canonical finite-size transition temperatures, for example, the peak location of the specific heat, do not depend on the kinetic contribution to the partition

function. In the canonical expectation values, the kinetic prefactor simply cancels. Here, however, we observe a finite-size difference in the transition temperature depending on whether we consider the kinetic contribution or not. Of course, the thermodynamic limit coincides. This is illustrated in the inset of Fig. 4a with a finite-size scaling of the transition temperature difference $\hat{\beta}_{\mathrm{eqa}}(N)-\beta_{\mathrm{eqa}}(N)$. It shows a prominent power law scaling of the form $\sim N^{-3/4}$, which interestingly is the same scaling as the inverse transition droplet volume. The finite-size difference arises from the convolution of an asymmetric energy probability distribution with the Maxwell–Boltzmann distribution, compare Fig. 1 and equation (8) in Methods section, which manifests in the geometric differences of the microcanonical inverse temperature and the enclosed areas in equation (2). It appears that correlations between the ensemble definitions account for compatible leading-order scaling corrections in equation (4), which further supports this ansatz and explains the observed difference.

For polymer aggregation in Fig. 4b, fits of equation (4) yield $\beta_0=0.64(2)$ and $\hat{\beta}_0=0.64(2)$ for $N_{\min}=14$ (guided by the inset) each with $Q\approx 0.8$, for reaction coordinate E and E_{p}, respectively. Qualitatively, the fit ansatz describes the data already well when including the smallest system sizes. Also the finite-size ensemble deviation in the inset shows a clear $N^{-3/4}$ trend for $N\geq 14$. Again, this is an indication for the analogy between cluster formation in polymer solutions and droplet formation in a particle gas.

Discussion

We have presented a shape-free approach to the estimation of canonical free-energy barriers in equilibrium droplet formation. The finite-size scaling is dominated by the predicted $N^{1/2}$ behaviour but we identified additional logarithmic corrections from precise numerical estimates. Somewhat surprisingly, the absolute free-energy barrier is sensitive to the consideration of the kinetic contribution. It is well known that the restriction to the conformational phase space does not influence finite-size transition points determined from canonical expectation values. These are evaluated on the level of the canonical partition function. The free-energy barrier and the associated equal-height or equal-area transition temperature, however, are determined from the energy probability distribution. Here the two formulations are related by a convolution with the Maxwell–Boltzmann distribution, which explains the finite-size differences. At the same time, the probability distributions are the integrands of the respective partition functions. In the end, this boils down to the trivial fact that equality of integrals does not imply equality of the integrands. This may become relevant once theoretical predictions and experimental measurements become precise enough. Still, a restriction to the conformational phase space retains intensive parameters in the thermodynamic limit. As a numerical advantage, considering the total energy as reaction coordinate leads to less fluctuations in the microcanonical partition function and canonical probability distribution, since the underlying convolution is a smoothing procedure of physical origin.

We provided evidence that the derived finite-size scaling of canonical droplet formation is applicable to cluster formation in dilute polymer solutions as well, despite the a priori non-trivial shape of the polymer cluster. This is a clear indication of an analogy between particle condensation and polymer aggregation. In particular, we showed that polymer clusters are in equilibrium with non-attached (free) polymers: an inhomogeneous or mixed phase of aggregate and solute polymers. This is intuitively clear when the polymers are interpreted as extended particles. The leading-order corrections then follow from the interplay between energy minimization by forming a local cluster and entropy maximization by retaining freely movable constituents. Of course, additional corrections should follow from the explicit geometry and internal behaviour of the constituents.

It is expected that the energy remains a suitable reaction coordinate for general nucleation-like mechanisms. In this case, generalized ensemble methods may unfold their full power. Moreover, our approach at fixed density provides the possibility for experiments to perform heating–cooling studies in order to probe transition rates. The presented results for polymer aggregation suggest that this approach may be generalized to studies of protein cluster formation[6]. In a wider scope, it may also find potential application for temperature-driven self-assembly[36,37], crystallization in phase-change materials[7–9] and glassy solids[10], dislocation nucleation[38] or the study of surface nanobubbles and nanodroplets[39]. Of course, experimental observations commonly include the formation of multiple clusters. Reasons for this include heterogeneities or impurities acting as nucleation seeds. We suppose that this leads to a local quasi-equilibrium on the respective length scales. Here a proper combination of the canonical droplet formation with the effect of nucleation seeds[40] seems to be a fruitful approach to a systematic understanding. With further developments, simulations may provide reliable estimates for finite-size systems and meet experiments on the nanometer scale.

Methods

Microcanonical ensembles. Recently, there has been some ambiguity with the definition of a 'microcanonical ensemble' in computer simulations[41]. This is a crucial aspect relevant for physical interpretations that appears to be unwittingly softened in the past decade. The microcanonical ensemble (NVE) describes an isolated system in which the number of constituents N, the volume V and the total energy E are conserved. Here the transfer of potential energy E_{p} into kinetic energy E_{k} and vice versa is a valid and relevant mechanism, where $E=E_{\mathrm{k}}+E_{\mathrm{p}}$. The microcanonical (Boltzmann) entropy is defined as $S(E)=k_{\mathrm{B}}\ln\Gamma(E)$, with the partition function $\Gamma(E)=\int\!\!\int \mathcal{D}x\,\mathcal{D}p\,\delta\big(E-\big[E_{\mathrm{p}}(x)+E_{\mathrm{k}}(p)\big]\big)$, where $\mathcal{D}x$ denotes the integration over state space and $\mathcal{D}p$ over momentum space.

The other common definition is the conformational microcanonical ensemble (NVE_{p}), describing instead a system with fixed potential energy E_{p}. The conformational microcanonical entropy is $\hat{S}(E_{\mathrm{p}})=k_{\mathrm{B}}\ln\Omega(E_{\mathrm{p}})$, where $\Omega(E_{\mathrm{p}})=\int\mathcal{D}x\,\delta\big(E_{\mathrm{p}}-E_{\mathrm{p}}(x)\big)$ is the density of states or the conformational microcanonical partition function. The consequences are drastic: a (physical) interpretation of energy transfer from potential to kinetic energy is no longer valid. This is natural for spin systems, where a kinetic contribution is not defined in the first place (but may be exploited for numerical purposes[42]). On the contrary, it is particularly relevant for situations in soft condensed matter, for example, for particles and polymers, where interpretations of energy transfer become natural. However, there are good reasons for this choice: $\Omega(E_{\mathrm{p}})$ is a fundamental property of statistical mechanics. It encodes the full information about the conformational space and allows for identification of (structural) phase transitions[30,31,43,44]. Furthermore, it may be exploited for reweighting techniques and flat-histogram Monte Carlo methods[18,45,46].

The relation between $\Gamma(E)$ and $\Omega(E_{\mathrm{p}})$ is given by a convolution with the kinetic energy contribution (see, for example, ref. 47): If momenta and positions are independent, one may separate the kinetic energy contribution $E_{\mathrm{k}}=\sum p_i^2/2m$, explicitly perform the momentum integration and obtain for N particles in three dimensions[48]

$$\Gamma(E)=\frac{(2\pi m)^{\frac{3N}{2}}}{\Gamma\left(\frac{3N}{2}\right)}\int_{-\infty}^{\infty}\mathrm{d}E_{\mathrm{p}}\,\Omega(E_{\mathrm{p}})\,(E-E_{\mathrm{p}})^{\frac{3N-2}{2}}\,\Theta(E-E_{\mathrm{p}}),\qquad(5)$$

where $\Gamma(\frac{3N}{2})$ is the Gamma function. We define $\Omega(E_{\mathrm{p}})=0\;\forall\;E_{\mathrm{p}}<E_{\mathrm{p,min}}$ in order to extend the integral over the full energy range $(-\infty,\infty)$. In this way, the total energy surface entropy $S(E)$ appears as a (weighted) potential energy volume entropy. Notice that, since all $\Omega(E_{\mathrm{p}})\geq 0$, the classical NVE entropy increases with E and the microcanonical inverse temperature $k_{\mathrm{B}}\beta(E)=\partial S(E)/\partial E$ cannot become negative, opposed to its conformational counterpart $k_{\mathrm{B}}\hat{\beta}(E_{\mathrm{p}})=\partial\hat{S}(E_{\mathrm{p}})/\partial E_{\mathrm{p}}$. This may be an interesting aspect for a recent debate on the correct definition of entropy when connected with the phenomenological thermodynamic entropy, for example, in refs 49–51 and references therein.

Numerically, we determine the microcanonical inverse temperatures as follows. In the conformational microcanonical ensemble, we have direct access to an estimate of $\ln\Omega(E_{\mathrm{p}})$ (see below) such that $\hat{\beta}(E_{\mathrm{p}})$ is obtained by a numerical five-point derivative. In the full microcanonical ensemble, we may estimate the inverse temperature in terms of microcanonical expectation values for N

independent particles

$$\langle O\rangle_E = \frac{\int \mathrm{d}E_\mathrm{p}\, O(E_\mathrm{p})\Omega(E_\mathrm{p})\left(E-E_\mathrm{p}\right)^{\frac{3N-2}{2}}\Theta(E-E_\mathrm{p})}{\int \mathrm{d}E_\mathrm{p}\,\Omega(E_\mathrm{p})\left(E-E_\mathrm{p}\right)^{\frac{3N-2}{2}}\Theta(E-E_\mathrm{p})}, \quad (6)$$

where the explicit prefactor in equation (5) cancels. Then we may express $\beta(E)=\partial \ln \Gamma(E)/\partial E = \frac{3N-2}{2}\left\langle \frac{1}{E-E_\mathrm{p}}\right\rangle_E$.

Canonical ensembles. The canonical ensemble is defined in terms of the partition function $Z_\beta = \int\int \mathcal{D}x\,\mathcal{D}p\, e^{-\beta E}$, where each phase-space point is weighted with the Boltzmann factor according to the total energy. Again, the kinetic part may be explicitly integrated for generic systems. Each degree of freedom contributes with a Gaussian integral, and one obtains for N particles,

$$Z_\beta = (2\pi m/\beta)^{3N/2}\hat{Z}_\beta, \quad (7)$$

where $\hat{Z}_\beta = \int \mathcal{D}x\; e^{-\beta E_\mathrm{p}}$ is the partition function of the conformational canonical ensemble. Both partition functions may be expressed as integrals in terms of the respective energies, namely, $Z_\beta = \int \mathrm{d}E\,\Gamma(E)e^{-\beta E}$ and $\hat{Z}_\beta = \int \mathrm{d}E_\mathrm{p}\,\Omega(E_\mathrm{p})e^{-\beta E_\mathrm{p}}$. The corresponding canonical energy probability distributions are defined as $P_\beta(E) = \Gamma(E)e^{-\beta E}/Z_\beta$ and $\hat{P}_\beta(E_\mathrm{p}) = \Omega(E_\mathrm{p})e^{-\beta E_\mathrm{p}}/\hat{Z}_\beta$.

We may now relate the two energy probability distributions by starting with the definition of $P_\beta(E)$ and inserting equations 5 and 7:

$$P_\beta(E) = \int_{-\infty}^{\infty} \mathrm{d}E_\mathrm{p}\hat{P}_\beta(E_\mathrm{p})\frac{\beta^{\frac{3N}{2}}}{\Gamma\left(\frac{3N}{2}\right)}\left(E-E_\mathrm{p}\right)^{\frac{3N-2}{2}}e^{-\beta\left(E-E_\mathrm{p}\right)}\Theta(E-E_\mathrm{p}). \quad (8)$$

We identify the latter part of the integrand as the N-particle Maxwell–Boltzmann distribution $P_\mathrm{MB}(x)$ and may write equation (8) as a convolution $P_\beta(E) = \left(\hat{P}_\beta \times P_\mathrm{MB}\right)(E)$.

Lennard-Jones particles. We consider a system of Lennard-Jones particles in a dimensionless periodic box of length L with fixed density $\rho = N/L^3 = 10^{-2}$. Mutual avoidance and short-range attraction are modelled by the 12–6 Lennard-Jones potential $V_\mathrm{LJ}(r) = 4\epsilon\left[(\sigma/r)^{12} - (\sigma/r)^6\right]$ with $\epsilon = 1$ and $\sigma = 2^{-1/6}$ such that $r_\mathrm{min} = 1$. For computational efficiency, the potential is cutoff at $r_c = 2.5\sigma$ and shifted by $-V_\mathrm{LJ}(r_c)$. System sizes range up to $N = 2{,}048$, which is competitive with state-of-the-art Molecular Dynamics simulations such as well-tempered metadynamics[52]. For the chosen density $\rho = 10^{-2}$, a system with 2,048 particles requires a box of linear dimension $L' \approx 59\, r'_\mathrm{min} = 59 \times 2^{1/6}\,\sigma'$. For argon, $\sigma' \approx 3.4$ Å such that $L' \approx 22.5$ nm is on the nanoscale. Of course, for a comparison to an experimental setup one should include both the explicit geometric constraints and the full Lennard-Jones potential.

Bead-spring polymers. The considered dilute polymer solution is modelled by N linear bead-spring polymers, consisting of 13 monomers each, again in a dimensionless periodic box with monomer density $\rho = 13N/L^3 = 10^{-2}$. Bonds are modelled between neighbouring monomers by the FENE potential $V_\mathrm{FENE}(r) = -(KR^2/2)\ln[1-(r-r_0)^2/R^2]$ with $K = 40$, $R = 0.3$ and $r_0 = 0.7$. Non-bonded monomers interact with the same Lennard-Jones potential as above but with $\sigma = r_0\, 2^{-1/6}$ such that $r_\mathrm{min} = r_0$[18–20]. The total number of monomers is $13N$, which yields $3 \times 13N$ total momentum degrees of freedom in equation (5) and successive relations. The bounded bond length $[r_0 - R,\ r_0 + R]$ from the FENE potential formally introduces constraints on these degrees of freedom. However, for practical applications in ordinary temperature ranges this effect is negligible and reweighting to the full microcanonical and canonical ensemble is feasible[41].

Multicanonical Monte Carlo simulations. Parallel multicanonical Monte Carlo simulations[53–58] allow us to efficiently sample the suppressed states, by iteratively adapting an auxiliary weight function $W(E_\mathrm{p})$ to yield a flat histogram $H(E_\mathrm{p})$. The final weight function is related to the density of states up to a multiplicative factor: $\Omega(E_\mathrm{p}) \propto H(E_\mathrm{p})/W(E_\mathrm{p})$. This gives direct access to microcanonical estimates and canonical expectation values at any temperature. Using equation (5), this even provides an estimate of $\Gamma(E)$. Monte Carlo updates for the particle case include short- and long-range particle displacements. For updates of the polymer configurations, we employed local single-monomer shifts, bond-rotation and double-bridging moves, as well as long-range polymer displacements We measure the conformational (potential) energy E_p and the number of particles in the largest cluster N_D as in ref. 29. Error bars are obtained by the Jackknife method[59,60].

Data availability. The data that support the findings of this study are available from the corresponding author upon request. The computer code required to generate the data as well as the analysis scripts that lead to our conclusions are available from the corresponding author upon reasonable request.

References

1. Feder, J., Russell, K. C., Lothe, J. & Pound, G. M. Homogeneous nucleation and growth of droplets in vapours. *Adv. Phys.* **15,** 111–178 (1966).
2. Oxtoby, D. W. Homogeneous nucleation: theory and experiment. *J. Phys. Condens. Matter* **4,** 7627–7650 (1992).
3. Kashchiev, D. *Nucleation: basic Theory with Applications* (Butterworth-Heinemann, 2000).
4. Auer, S. & Frenkel, D. Prediction of absolute crystal-nucleation rate in hard-sphere colloids. *Nature* **409,** 1020–1023 (2001).
5. Sear, R. P. Nucleation: theory and applications to protein solutions and colloidal suspensions. *J. Phys. Condens. Matter* **19,** 033101 (2007).
6. Stradner, A. *et al.* Equilibrium cluster formation in concentrated protein solutions and colloids. *Nature* **432,** 492–495 (2004).
7. Kalb, J. A., Spaepen, F. & Wuttig, M. Kinetics of crystal nucleation in undercooled droplets of Sb- and Te-based alloys used for phase change recording. *J. Appl. Phys.* **98,** 054910 (2005).
8. Wuttig, M. & Yamada, N. Phase-change materials for rewriteable data storage. *Nat. Mater.* **6,** 824–832 (2007).
9. Lee, T. H. & Elliott, S. R. Ab initio computer simulation of the early stages of crystallization: application to $Ge_2\,Sb_2\,Te_5$ phase-change materials. *Phys. Rev. Lett.* **107,** 145702 (2011).
10. Lee, B.-S. *et al.* Observation of the role of subcritical nuclei in crystallization of a glassy solid. *Science* **326,** 980–984 (2009).
11. Langer, J. S. Theory of the condensation point. *Ann. Phys. NY* **41,** 108–157 (1967).
12. Goodmann, A. L., Kapusta, J. I. & Mekjian, A. Z. Liquid-gas phase instabilities and droplet formation in nuclear reactions. *Phys. Rev. C* **30,** 851–865 (1984).
13. Hansen, N. & van Gunsteren, W. F. Practical aspects of free-energy calculations: a review. *J. Chem. Theory Comput.* **10,** 2632–2647 (2014).
14. Schrader, M., Virnau, P. & Binder, K. Simulation of vapor-liquid coexistence in finite volumes: a method to compute the surface free energy of droplets. *Phys. Rev. E* **79,** 061104 (2009).
15. Hale, B. N. & Thomason, M. Scaled vapor-to-liquid nucleation in a Lennard-Jones system. *Phys. Rev. Lett.* **105,** 046101 (2010).
16. Tanaka, K. K., Diemand, J., Angélil, R. & Tanaka, H. Free energy of cluster formation and a new scaling relation for the nucleation rate. *J. Chem. Phys.* **140,** 194310 (2014).
17. Statt, A., Virnau, P. & Binder, K. Finite-size effects on liquid-solid phase coexistence and the estimation of crystal nucleation barriers. *Phys. Rev. Lett.* **114,** 026101 (2015).
18. Zierenberg, J., Marenz, M. & Janke, W. Dilute semiflexible polymers with attraction: collapse, folding and aggregation. *Polymers* **8,** 333 (2016).
19. Zierenberg, J., Mueller, M., Schierz, P., Marenz, M. & Janke, W. Aggregation of theta-polymers in spherical confinement. *J. Chem. Phys.* **141,** 114908 (2014).
20. Zierenberg, J. & Janke, W. From amorphous aggregates to polymer bundles: the role of stiffness on structural phases in polymer aggregation. *Europhys. Lett.* **109,** 28002 (2015).
21. Binder, K. & Kalos, M. H. 'Critical clusters' in a supersaturated vapor: theory and Monte Carlo simulation. *J. Stat. Phys.* **22,** 363–396 (1980).
22. Furukawa, H. & Binder, K. Two-phase equilibria and nucleation barriers near a critical point. *Phys. Rev. A* **26,** 556–566 (1982).
23. Biskup, M., Chayes, L. & Kotecký, R. On the formation/dissolution of equilibrium droplets. *Europhys. Lett.* **60,** 21–27 (2002).
24. Biskup, M., Chayes, L. & Kotecký, R. Critical region for droplet formation in the two-dimensional Ising model. *Commun. Math. Phys.* **242,** 137–183 (2003).
25. Neuhaus, T. & Hager, J. S. 2D crystal shapes, droplet condensation, and exponential slowing down in simulations of first-order phase transitions. *J. Stat. Phys.* **113,** 47–83 (2003).
26. Binder, K. Theory of the evaporation/condensation transition of equilibrium droplets in finite volumes. *Physica A* **319,** 99–114 (2003).
27. Nußbaumer, A., Bittner, E., Neuhaus, T. & Janke, W. Monte Carlo study of the evaporation/condensation transition of Ising droplets. *Europhys. Lett.* **75,** 716–722 (2006).
28. Nußbaumer, A., Bittner, E. & Janke, W. Monte Carlo study of the droplet formation-dissolution transition on different two-dimensional lattices. *Phys. Rev. E* **77,** 041109 (2008).
29. Zierenberg, J. & Janke, W. Exploring different regimes in finite-size scaling of the droplet condensation-evaporation transition. *Phys. Rev. E* **92,** 012134 (2015).
30. Gross, D. H. E. *Microcanonical Thermodynamics* (World Scientific, 2001).
31. Janke, W. Canonical versus microcanonical analysis of first-order phase transitions. *Nucl. Phys. B (Proc. Suppl.)* **63 A-C,** 631–633 (1998).
32. Ryu, S. & Cai, W. Validity of classical nucleation theory for Ising models. *Phys. Rev. E* **81,** 030601R (2010).
33. Nußbaumer, A., Bittner, E. & Janke, W. Free-energy barrier at droplet condensation. *Prog. Theor. Phys. Suppl.* **184,** 400–414 (2010).
34. Prestipino, S., Laio, A. & Tosatti, E. Systematic improvement of classical nucleation theory. *Phys. Rev. Lett.* **108,** 225701 (2012).
35. Prestipino, S., Laio, A. & Tosatti, E. A fingerprint of surface-tension anisotropy in the free-energy cost of nucleation. *J. Chem. Phys.* **140,** 094501 (2014).

36. Jonkheijm, P., van der Schoot, P., Schenning, A. P. H. J. & Meijer, E. W. Probing the solvent-assisted nucleation pathway in chemical self-assembly. *Science* **313,** 80–83 (2006).
37. Huisman, B. A. H., Bolhuis, P. G. & Fasolino, A. Phase transition to bundles of flexible supramolecular polymers. *Phys. Rev. Lett.* **100,** 188301 (2008).
38. Ryu, S., Kang, K. & Cai, W. Entropic effect on the rate of dislocation nucleation. *Proc. Natl Acad. Sci. USA* **108,** 5174–5178 (2011).
39. Lohse, D. & Zhang, X. Surface nanobubbles and nanodroplets. *Rev. Mod. Phys.* **87,** 981–1035 (2015).
40. Cacciuto, A., Auer, S. & Frenkel, D. Onset of heterogeneous crystal nucleation in colloidal suspensions. *Nature* **428,** 404–406 (2004).
41. Schierz, P., Zierenberg, J. & Janke, W. Molecular dynamics and Monte Carlo simulations in the microcanonical ensemble: quantitative comparison and reweighting techniques. *J. Chem. Phys.* **143,** 134114 (2015).
42. Martin-Mayor, V. Microcanonical approach to the simulation of first-order phase transitions. *Phys. Rev. Lett.* **98,** 137207 (2007).
43. Kastner, M. & Pleimling, M. Microcanonical phase diagrams of short-range ferromagnets. *Phys. Rev. Lett.* **102,** 240604 (2009).
44. Schnabel, S., Seaton, D. T., Landau, D. P. & Bachmann, M. Microcanonical entropy inflection points: key to systematic understanding of transitions in finite systems. *Phys. Rev. E* **84,** 011127 (2011).
45. Janke, W. in *Order, Disorder and Criticality: advanced Problems of Phase Transition Theory* Vol. 3 (ed. Holovatch, Y.) 93–166 (World Scientific, 2012).
46. Janke, W. & Paul, W. Thermodynamics and structure of macromolecules from flat-histogram Monte Carlo simulations. *Soft Matter* **12,** 642–657 (2016).
47. Labastie, P. & Whetten, R. L. Statistical thermodynamics of the cluster solid-liquid transition. *Phys. Rev. Lett.* **65,** 1567–1570 (1990).
48. Calvo, F., Neirotti, J. P., Freeman, D. L. & Doll, J. D. Phase changes in 38-atom Lennard-Jones clusters. II. A parallel tempering study of equilibrium and dynamic properties in the molecular dynamics and microcanonical ensembles. *J. Chem. Phys.* **112,** 10350–10357 (2000).
49. Dunkel, J. & Hilbert, S. Consistent thermostatistics forbids negative absolute temperatures. *Nat. Phys.* **10,** 67–72 (2014).
50. Hilbert, S., Hänggi, P. & Dunkel, J. Thermodynamic laws in isolated systems. *Phys. Rev. E* **90,** 062116 (2014).
51. Swendsen, R. H. & Wang, J. S. Gibbs volume entropy is incorrect. *Phys. Rev. E* **92,** 020103(R) (2015).
52. Salvalaglio, M., Tiwary, P., Maggioni, G. M., Mazzotti, M. & Parrinello, M. Overcoming timescale and finite-size limitations to compute nucleation rates from small scale well tempered metadynamics simulations. *J. Chem. Phys.* **145,** 211925 (2016).
53. Berg, B. A. & Neuhaus, T. Multicanonical algorithms for first order phase transitions. *Phys. Lett. B* **267,** 249–253 (1991).
54. Berg, B. A. & Neuhaus, T. Multicanonical ensemble: a new approach to simulate first-order phase transitions. *Phys. Rev. Lett.* **68,** 9–12 (1992).
55. Janke, W. Multicanonical simulation of the two-dimensional 7-state Potts model. *Int. J. Mod. Phys. C* **03,** 1137–1146 (1992).
56. Janke, W. Multicanonical Monte Carlo simulations. *Physica A* **254,** 164–178 (1998).
57. Zierenberg, J., Marenz, M. & Janke, W. Scaling properties of a parallel implementation of the multicanonical algorithm. *Comput. Phys. Commun.* **184,** 1155–1160 (2013).
58. Zierenberg, J., Wiedenmann, M. & Janke, W. Application of the parallel multicanonical method to lattice gas condensation. *J. Phys. Conf. Ser.* **510,** 012017 (2014).
59. Efron, B. *The Jackknife, the Bootstrap and Other Resampling Plans* (Society for Industrial and Applied Mathematics, 1982).
60. Young, P. *Everything You Wanted to Know About Data Analysis and Fitting but Were Afraid to Ask*. Springer Briefs in Physics (Springer International Publishing, 2015).

Acknowledgements

The project was funded by the European Union, the Free State of Saxony and the Deutsche Forschungsgemeinschaft (DFG) under Grant No. JA 483/31-1 and Sonderforschungsbereich/Transregio SFB/TRR 102 (Project B04). We gratefully acknowledge the computing time provided by the John von Neumann Institute for Computing (NIC) on the supercomputer JURECA at Jülich Supercomputing Centre (JSC) under Grant No. HLZ24. Part of this work has been financially supported by the Leipzig Graduate School of Natural Sciences 'BuildMoNa' and by the Deutsch-Französische Hochschule (DFH-UFA) through the Doctoral College '$\mathbb{L}^4$' under Grant No. CDFA-02-07.

Author contributions

All authors contributed equally to the theory and J.Z. performed the simulations. J.Z. and W.J. analysed the data and wrote the paper. All authors discussed the results and commented on the manuscript.

Additional information

Competing financial interests: The authors declare no competing financial interests.

Reprints and permission information is available online at http://npg.nature.com/reprintsandpermissions/

How to cite this article: Zierenberg, J. *et al.* Canonical free-energy barrier of particle and polymer cluster formation. *Nat. Commun.* **8**, 14546 doi: 10.1038/ncomms14546 (2017).

Publisher's note: Springer Nature remains neutral with regard to jurisdictional claims in published maps and institutional affiliations.